

# MODELING OF AUSTENITIC TRIP-STEELS AT SMALL SCALES – A MEAN-FIELD HOMOGENIZATION APPROACH

S. PRÜGER\* AND B. KIEFER\*

\* TU Bergakademie Freiberg  
Institute of Mechanics and Fluid Dynamics  
Lampadiusstrasse 4, 09599 Freiberg, Germany  
e-mail: Stefan.Prueger@imfd.tu-freiberg.de, web page:  
<https://tu-freiberg.de/fakult4/imfd/fkm>

**Key words:** Crystal Plasticity, Mean-Field Homogenization, Finite Deformation, Inhomogeneous Inhomogeneity, Regularized Transformation Velocity Gradient

**Abstract.** A finite deformation mean-field homogenization approach is proposed based on an extended Mori-Tanaka scheme that incorporates additional eigenvelocity gradients associated with microstructural changes in austenitic steels such as twinning or solid-solid phase transformation. The deformation of the individual phases is described by a finite strain, hyperelastic and single crystal plasticity model, which is fully anisotropic and captures strong mutual interactions of individual slip systems. The resulting mean-field model is employed in the simulation of homogeneous deformation states with a prescribed microstructure evolution at the material point level, where a strong interaction between phase transformation and plasticity is observed in the individual phases.

## 1 INTRODUCTION

The constitutive modeling of high-alloyed, metastable austenitic steels, which show the Transformation-Induced Plasticity (TRIP)-effect, is a challenging task, because depending on chemical composition, temperature, load case and loading rate, a variety of different deformation mechanisms is observed [1]. In particular, the face-centered austenite deforms via dislocation glide, twinning, stacking fault formation and stress-assisted / strain-induced martensitic phase transformation. Within the last decades, a large number of constitutive models were proposed to capture these phenomena at the macroscopic scale assuming a polycrystalline microstructure, cf. [2, 3] for phenomenological and [4, 5] for micromechanical models. At the single crystal scale, the different deformation mechanisms are more naturally incorporated, but the discrete and anisotropic nature of the transformation, slip and twinning systems renders such approaches still quite challenging, at least from the numerical point of view. Common extensions of crystal plasticity models employ a superposition of the different deformation mechanisms [6, 7], in which for all the mechanisms the same stress measure is chosen as driving force. It may therefore be interpreted as a Reuss-type homogenization approach. Additionally, crystal plasticity models have been generalized by extending the multiplicative decomposition of the deformation

gradient and introducing additional intermediate configurations associated with each of the mechanisms [8, 9]. Neither of the two approaches incorporates information from the underlying microstructure other than the volume fractions of for instance transformed or twinned domains. Furthermore, in order to account for the changes in the elastic properties due to the presence of these transformed or twinned domains [6, 9], the equality of the elastic deformation measure within these domains and the embedding austenite is postulated. Despite the fact that such an assumption allows for an efficient incorporation of the important aspect of changing elastic behavior upon twinning or phase transformation, it is not consistent with common micromechanics approaches and certainly does not hold for a general arrangement of twinned/transformed domains, in particular if these domains are characterized by anisotropic elastic properties.

On the contrary, micromechanics approaches offer the advantage that features of the microstructure beyond the volume fraction, like for instance the particle shape, the aspect ratio of inclusions or the orientation distribution of elongated inclusions can be accounted for and that sound scale transition rules are available, which prescribe how the macroscopic deformation is projected into particular domains of a heterogeneous material. Approaches in which single crystal plasticity models are combined with homogenization schemes commonly aim for a more accurate description of the polycrystalline behavior, cf. [10, 11] for an application of a self-consistent scheme that accounts for transformation induced eigenstrains, in the context of finite deformations, while in [12] a small deformation framework is employed in a similar manner.

The current contribution also utilizes a homogenization scheme in connection with a finite strain single crystal plasticity model, but the aim is to improve the predictions at the single crystal scale and refine existing models employed in multi-scale approaches [13].

Throughout the paper, the following notation is used. Scalar variables  $a$  are denoted in italic, while parameters  $a$  are shown upright. Vectors  $\mathbf{a}$  and second order tensors  $\mathbf{A}$  are distinguished by italic and upright bold symbols, while fourth order tensors are expressed as  $\mathbb{A}$ . Furthermore, the dyadic product of two vectors gives a second order tensor  $\mathbf{A} = \mathbf{a} \otimes \mathbf{b}$  and the square product between second order tensors is computed as  $\mathbb{A} = \mathbf{A} \boxtimes \mathbf{B} = A_{ik} B_{jl} \mathbf{e}_i \mathbf{e}_j \mathbf{e}_k \mathbf{e}_l$  in Cartesian coordinates.

## 2 MEAN-FIELD HOMOGENIZATION ACCOUNTING FOR INHOMOGENEOUS INHOMOGENEITIES

Analytical homogenization methods to a great extent employ classic results from Eshelby's ellipsoidal inclusion problem [14] to estimate the overall properties of an heterogeneous material. Herein, the heterogeneous material is replaced by a fictitious homogeneous comparison material that experiences a suitably chosen eigenstrain field. Following the terminology of [15, p.77ff], the latter is also referred to as an inclusion, whereas a domain with properties different from the embedding material is called an inhomogeneity. The described procedure is perfectly suitable for composite materials, in which the composition is fixed and the arrangement of the individual constituents only changes if finite deformations and/or damage and fracture are considered. On the contrary, in materials

undergoing phase transformation the situation is more complex, as new product phases evolve upon the change of external stimuli, e.g. deformation, temperature, magnetic field, etc., from the parent phase. In addition to the different properties of parent and product phase, the phase transformation is often associated with a characteristic transformation strain. A generalization of Eshelby's inclusion problem that accounts for these additional strain contributions is described in [15, p.88ff] in the framework of small deformations. Therein, a domain, whose properties are different from the embedding material and which experiences additional eigenstrains, is referred to as an inhomogeneous inhomogeneity. In the current contribution, the procedure mentioned above is translated to a finite deformation framework, by a proper choice of kinematic and kinetic variables. In [16], the velocity gradient is proposed as a suitable kinematic variable to solve a rate-type Eshelby inclusion problem in the framework of finite deformations without considering contributions from additional transformation velocity gradients. Adopting this proposal and employing the assumption that the inhomogeneous inhomogeneity is embedded into the matrix experiencing an average velocity gradient  $\mathbf{L}_{\text{mat}}$ , see [15, p.163ff.] and [17] for an equivalent assumption under small strains, one obtains the relation

$$\bar{\mathbf{L}} = [f_0 \mathbb{B} + (1 - f_0) \mathbb{I}] : \mathbf{L}_{\text{mat}} + f_0 [\mathbb{I} + \mathbb{B} : [\mathbb{P} : \mathbb{F}_{\text{mat}} - \mathbb{I}]] : \mathbf{L}^{\text{tr}} \quad (1)$$

together with the relation for the average velocity gradients in a two-phase material

$$\bar{\mathbf{L}} = f_0 \mathbf{L}_{\text{incl}} + (1 - f_0) \mathbf{L}_{\text{mat}} . \quad (2)$$

Herein, the overall velocity gradient, the transformation velocity gradient and the average velocity gradient in the inhomogeneity are denoted as  $\bar{\mathbf{L}}$ ,  $\mathbf{L}^{\text{tr}}$  and  $\mathbf{L}_{\text{incl}}$ , respectively, while  $f_0$  is the volume fraction of the inhomogeneity. Furthermore,  $\mathbb{B}$  is termed the "strain" concentration tensor and relates the average velocity gradients in the inhomogeneity and in the matrix. According to [18], it is considered the finite strain extension of the concentration tensor introduced by Mori-Tanaka [17]. It is determined from

$$\mathbb{B} = [\mathbb{I} + \mathbb{P} : [\mathbb{F}_{\text{incl}} - \mathbb{F}_{\text{mat}}]]^{-1} , \quad (3)$$

in which the Hill tensor  $\mathbb{P}$ , specified in detail e.g. in [16, 19, 20] depends on the current geometry of the inhomogeneity and the constitutive tangent  $\mathbb{F}_{\text{mat}}$  of the matrix material. The latter emerges from a rate-type description of the constitutive model and connects the rate of the nominal stress  $\dot{\mathbf{n}}$  and the velocity gradient, i.e.

$$\dot{\mathbf{n}} = \mathbb{F} : \mathbf{L} . \quad (4)$$

This type of constitutive description also plays a key role in the generalization of mean-field homogenization approaches from small to finite deformations, cf. [21, 16, 18]. Here, the approach proposed in [21] is adopted, together with the assumption that the current configuration is taken as the reference configuration, which allows one to express the rate of the nominal stress in terms of the Lie derivative of the Kirchhoff stress as

$$\dot{\mathbf{n}} = \mathcal{L}(\boldsymbol{\tau}) + \boldsymbol{\tau} \cdot \mathbf{L}^{\text{T}} \quad (5)$$

and establishes the connection between the nominal and the spatial tangent operators as

$$\mathbb{F} = \mathbb{c} + \boldsymbol{\tau} \boxtimes \mathbf{I} . \quad (6)$$

In contrast to [21], the overall stress is not obtained by integration of the rate-type constitutive equations, but by averaging the Kirchhoff stress in the individual phases, obtained from the hyperelastic-plastic material models introduced in Section 3, over the initial volume of the heterogeneous material as

$$\bar{\boldsymbol{\tau}} = [f_0 \boldsymbol{\tau}_{\text{incl}} + (1 - f_0) \boldsymbol{\tau}_{\text{mat}}] \frac{\bar{J}}{f_0 J_{\text{incl}} + (1 - f_0) J_{\text{mat}}} \quad (7)$$

Herein, an estimate of the average volume change in the individual phases of the heterogeneous material [18] is included in the averaging process.  $\bar{J}$ ,  $J_{\text{incl}}$  and  $J_{\text{mat}}$  denote the determinant of the overall deformation gradient and the determinant of the deformation gradient in the individual phases, respectively. These deformation gradients are obtained by integrating the velocity gradient, determined from the system (1) and (2). They are also employed in the evaluation of the hyperelastic-plastic constitutive models.

Furthermore, the overall nominal tangent is obtained as the average of the individual tangents, i.e.

$$\bar{\mathbb{F}} = \mathbb{F}_{\text{incl}} + (1 - f_0) [\mathbb{F}_{\text{mat}} - \mathbb{F}_{\text{incl}}] : \frac{\partial \mathbf{L}_{\text{mat}}}{\partial \bar{\mathbf{L}}} , \quad (8)$$

employing (4) and (2). Note that, the implicit function theorem is applied to (1) to compute the derivative of the velocity gradient in the matrix with respect to the overall velocity gradient numerically by means of the complex step derivative [22]. Taking into account the identity that the average of the product of nominal stress and deformation rate decomposes into the product of averages under prescribed uniform boundary conditions [16] and considering the choice that the current configuration is taken as reference, a relation identical to (5) can also be established for the overall quantities. Thus, the overall spatial tangent can be deduced and takes the form

$$\bar{\mathbb{c}} = \bar{\mathbb{F}} - \bar{\boldsymbol{\tau}} \boxtimes \mathbf{I} . \quad (9)$$

In order to complete the model, a description of the stress-free transformation velocity gradient is required, which may be due to diffusion, chemical reactions or solid-solid phase transformations. In the current contribution, the transformation velocity gradient is associated with the diffusionless martensitic transformation in high-alloyed steels from face-centered austenite to body-centered martensite. At the single crystal scale, crystallography based theories are typically employed to derive the kinematics associated with this transformation, cf. [23, 24, 25], which provides the corresponding deformation gradient that transforms the crystal lattice. Furthermore, it is commonly assumed [13, 26, 27, 12] that this deformation gradient is present as soon as martensite nuclei appears, i.e. the deformation gradient is prescribed by a step function. Although this approach is physically sound, it is not applicable in the formulation (1) without modification, because the

jump in the deformation renders the associated velocity gradient infinite. Therefore, the non-smooth activation of the deformation gradient is regularized by

$$\mathbf{F}^{\text{tr}} = \mathbf{I} + \sum_{\text{I}} \frac{\xi_{\text{I}}}{f_{\text{m}}} g(\xi_{\text{I}}) \mathbf{M}_{\text{I}} \otimes \mathbf{N}_{\text{I}}, \quad (10)$$

in which  $\mathbf{M}_{\text{I}}$ ,  $\mathbf{N}_{\text{I}}$ ,  $\xi_{\text{I}}$  and  $f_{\text{m}}$  denote the shape deformation vector, the habit plane normal, the volume fraction of the martensite variant I and the martensite volume fraction, respectively, while  $g(\xi_{\text{I}})$  is a nonnegative, continuous, monotonically increasing function with  $g(0) = 0$  and  $g(1) = 1$ , that regularizes the step function. In the subsequent computations, presented in Section 4.2, the function

$$g(\xi_{\text{I}}) = 1 - \exp(-c \xi_{\text{I}}) \quad (11)$$

is chosen, in which  $c$  controls the initial slope. The transformation velocity gradient is obtained from  $\mathbf{L}^{\text{tr}} = \dot{\mathbf{F}}^{\text{tr}} \cdot \mathbf{F}^{\text{tr}}$ .

### 3 MATERIAL MODEL OF INDIVIDUAL PHASES

The constitutive response of the individual, single-crystalline phases is described by means of a finite deformation crystal plasticity model, which is based on the multiplicative split of the deformation gradient

$$\mathbf{F} = \mathbf{F}^{\text{e}} \cdot \mathbf{F}^{\text{p}} \quad (12)$$

into an elastic and a plastic part. The former is used to determine the second Piola-Kirchhoff stress in the intermediate configuration from the hyperelastic relation

$$\hat{\mathbf{S}} = 2 \frac{\partial \psi^{\text{e}}(\mathbf{C}^{\text{e}})}{\partial \mathbf{C}^{\text{e}}} = 2 \underbrace{\frac{\partial \tilde{\psi}^{\text{e}}}{\partial \mathbf{E}^{\text{m}}}}_{\mathbf{T}} : \frac{\partial \mathbf{E}^{\text{m}}}{\partial \mathbf{C}^{\text{e}}}, \quad (13)$$

in which the right Cauchy-Green tensor is computed as  $\mathbf{C}^{\text{e}} = \mathbf{F}^{\text{eT}} \cdot \mathbf{F}^{\text{e}}$ , while  $\mathbf{E}^{\text{m}}$  and  $\mathbf{T}$  denote the generalized strain tensor of Seth-Hill type and the stress dual to the Seth-Hill strain, respectively. The elastic part of the free-energy  $\tilde{\psi}^{\text{e}}$  employs a quadratic form of the Seth-Hill strain and also incorporates the cubic symmetry of the crystal, see [28] for further details.

The evolution of the plastic part of the deformation gradient is described by the associative multi-surface flow rule

$$\dot{\mathbf{F}}^{\text{p}} \cdot \mathbf{F}^{\text{p}-1} = \sum_{\alpha}^{\text{N}_{\text{slip}}} \dot{\lambda}_{\alpha} \mathbf{S}_{\alpha} \otimes \mathbf{N}_{\alpha}, \quad (14)$$

where  $\mathbf{S}_{\alpha}$  and  $\mathbf{N}_{\alpha}$  denote the slip direction and slip plane normal, respectively. In the face-centered austenite (fcc), the family of primary  $\langle 110 \rangle \{111\}$  slip systems is considered, while in the body-centered martensite (bcc), two families of slip systems, namely the  $\langle 111 \rangle \{110\}$  systems and the  $\langle 111 \rangle \{112\}$  systems, are taken into account. Differentiating between positive and negative slip directions of a given slip system gives rise to a total number of

slip systems  $N_{\text{slip}} = 24$  in the fcc structure, whereas for the bcc crystal  $N_{\text{slip}} = 48$ . The Lagrange multipliers  $\dot{\lambda}_\alpha$ , characterizing the plastic slip rate on the different slip systems, are determined from the KKT conditions

$$\dot{\lambda}_\alpha \geq 0, \quad \Phi_\alpha \leq 0 \quad \dot{\lambda}_\alpha \Phi_\alpha = 0, \quad (15)$$

where the repeated index  $\alpha$  does not imply a summation. The yield function, associated with each of the slip systems, takes the form

$$\Phi_\alpha = \mathbf{M} : [\mathbf{S}_\alpha \otimes \mathbf{N}_\alpha] - Y_0 - Y_\alpha(\varepsilon_\beta). \quad (16)$$

Herein, the Mandel stress is related to the second Piola-Kirchhoff stress as  $\mathbf{M} = \mathbf{C}^e \cdot \widehat{\mathbf{S}}$  and  $Y_\alpha(\varepsilon_\beta)$  describes the hardening associated with the slip system  $\alpha$ . In particular, it includes self- and latent hardening effects by means of a six-parameter interaction matrix ( $h_{\alpha\beta}$ ) and the saturation-type, phenomenological hardening function [29]

$$Y_\alpha(\varepsilon_\beta) = \Delta Y \sum_\beta h_{\alpha\beta} [1 - \exp(-h \varepsilon_\beta)]. \quad (17)$$

In the case of the bcc crystal, where the dislocation slip along the dense  $\langle 111 \rangle$  directions involves several slip planes, the two-parameter interaction matrix introduced by Asaro [30] is employed. The interaction of different slip systems is only accounted for among the systems of the same family, while the interaction of systems stemming from different families is neglected. Finally, it is remarked that the hardening variables  $\varepsilon_\alpha$  are determined from the temporal integration of the corresponding Lagrange multiplier. For further details regarding the derivation of the model and the implementation of the rate-independent model by means of an Augmented-Lagrangian formulation, the interested reader is referred to [31, 32].

## 4 RESULTS

### 4.1 Parameter estimation of individual phases

In order to obtain meaningful results from the mean-field homogenization approach described in Section 2, the parameters in the constitutive models employed for the individual phases have to be estimated. Therefore, the experimentally measured response of an AISI 316L single crystal [33] is taken as a reference for the austenitic phase, where it is assumed that the evolution of the microstructure at room temperature, like the formation of stacking faults and twins, has at least initially a minor influence on the hardening behavior. Thus, the estimation of the hardening parameters of the crystal plasticity model from the initial portion of the measured stress-strain curve corresponds to a reasonable description of a stable austenitic single crystal. Similarly, experimental data obtained from bcc  $\alpha$ -iron single crystals [34] is used to estimate the hardening parameters employed in the crystal plasticity model of the martensitic phase. Due to the fact that  $\alpha$ -iron and the martensitic phase in a metastable TRIP-steel both possess a bcc crystal structure, it is furthermore assumed that the addition of typical alloying elements, like chromium, nickel,

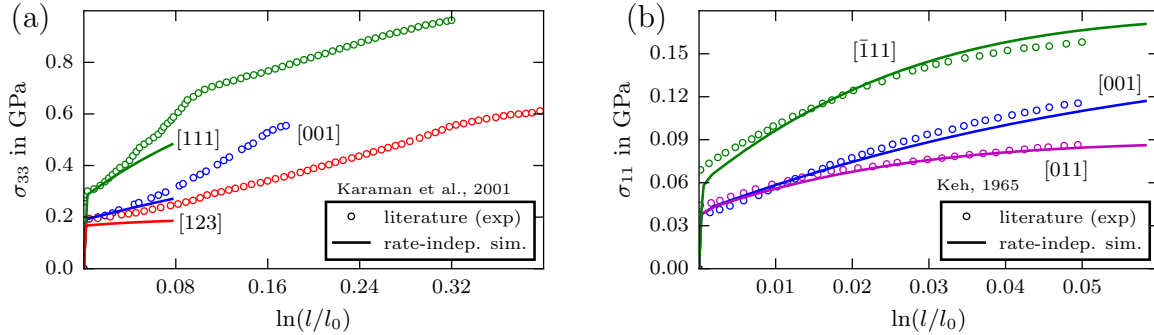


**Figure 1:** Comparison of the experimentally measured and simulated response of a single crystal under uniaxial tension along different crystal orientations: (a) AISI 316L and (b)  $\alpha$ -iron. The experimental data is taken from the literature.

manganese and carbon, only increases the initial yield stress of the martensitic phase and does not alter its hardening behavior significantly. Of course, more realistic parameter estimation might be obtained from nanoindentation experiments [35, 36], which is however beyond the scope of the current contribution. The results of the simulated uniaxial tensile tests along different crystal orientations are depicted in Fig. 1 together with the experimental data points from the literature. Within the simulations, spatially homogeneous deformation states are assumed, which is a reasonable assumption at least for the highly symmetric crystal orientations and allows for efficient simulations at the material point level. The material parameters associated with the two phases are presented in Table 1.

phase	$C_{11}$	$C_{12}$	$C_{44}$	$Y_0$	$h_1$	$h_2$	$h_3$	$h_4$	$h_5$	$h_6$
$\gamma$	204.6 GPa	137.7 GPa	126.2 GPa	78.0 MPa	1.0	1.0	0.6	12.3	1.6	1.3
	$h$	$m$	$\Delta Y$							
	10.0	0.0	8.0 MPa							
phase	$C_{11}$	$C_{12}$	$C_{44}$	$Y_0$	$h_1$	$h_2 = h_3 = h_4 = h_5 = h_6$				
$\alpha'$	231.4 GPa	134.5 GPa	116.3 GPa	224.4 MPa	1.0	1.4				
	$h$	$m$	$\Delta Y$							
	60.0	0.0	10.0 MPa							

**Table 1:** Material parameters of the austenitic phase ( $\gamma$ ) and martensitic phase ( $\alpha'$ ). The elastic coefficients are taken from [37, 38] and the parameters of the interaction matrix are adopted from [39]. Note that the initial yield stress is increased to account for contributions from alloying elements in martensite and an initial yield stress of  $Y_0 = 17.87$  MPa is determined for pure  $\alpha$ -iron.

## 4.2 Two-phase composite with evolving microstructure

The micromechanical model, described in Section 2, is employed in connection with the calibrated single crystal plasticity model for the austenitic and the martensitic phase to investigate the effect of the phase transformation onto the elastic-plastic deformation of the individual phases. Therefore, a uniaxial tension and a uniaxial compression test along the [010] direction of the austenite is simulated, prescribing the initial orientations

such that the principle axes of the crystal lattice of both phases are aligned with the axes of the global coordinate system. The shape deformation vector and the habit plane normal associated with 24 transformation systems are adopted from [13]. Furthermore, the evolution of 8 favorable variants that develop upon loading is prescribed as a function of the overall deformation. It is also taken from [13] and illustrated in Fig. 2 (b) and 3 (b). In the two-phase model at hand, it is additionally assumed that all the variants evolve simultaneously within the initially spherical, martensitic inhomogeneity. The resulting

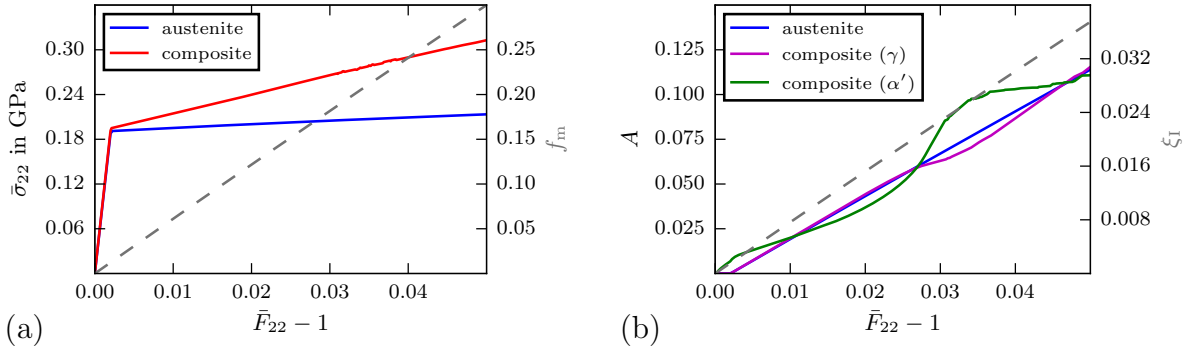


**Figure 2:** Comparison of the material response under uniaxial tension. (a) true stress-nominal strain curve of the two-phase composite material and the pure austenite and (b) evolution of the accumulated plastic slip  $A = \sum_{\alpha} \varepsilon_{\alpha}$  in the individual phases of the composite material and the pure austenite.

stress-strain curves are depicted in Fig. 2 (a) and 3 (a). Comparing the results with the ones for the pure austenite, a strengthening due to the evolving microstructure and the transformation induced deformation is clearly visible. Note that the prescribed evolution of the martensite variants possesses an asymmetry, i.e. more martensite is formed in tension than in compression at the same absolute value of nominal strain. This asymmetry can also be observed in the strengthening, although the absolute values of stress only differ slightly. On the contrary, the evolution of the accumulated plastic slip  $A$  in the individual phases varies significantly in tension and compression. While during the initial stage of the test, the evolution of the accumulated plastic slip in the austenitic phase of the two-phase material closely follows the evolution of the pure austenite, due to the small martensitic volume fraction, the martensitic phase shows a strong increase in the accumulated plastic slip, which is even more pronounced in compression than in tension and stems from the accommodation of the transformation induced deformation. As the transformation deformation gradient  $\mathbf{F}^{\text{tr}}$  reaches its asymptotic value at  $\xi_1 \approx 0.01$ , plastic slip activity in martensite drops to that of the austenite or even below in uniaxial tension. Within the strain range  $|\bar{F}_{22} - 1| \in [0.023, 0.042]$ , the deformation of martensite in the compression test is almost entirely accommodated elastically, thus causing additional plastic deformation in the austenite. Under uniaxial tension, this trend is reversed and more plastic slip is observed in the martensite, while the plastic slip activity in the austenitic phase of the two-phase material decreases below that of the pure austenite. Thus, one can conclude that there is a strong coupling of the plastic flow in the individual phases, their contribution to the overall straining changes dynamically and is even sensitive to the direction of loading.

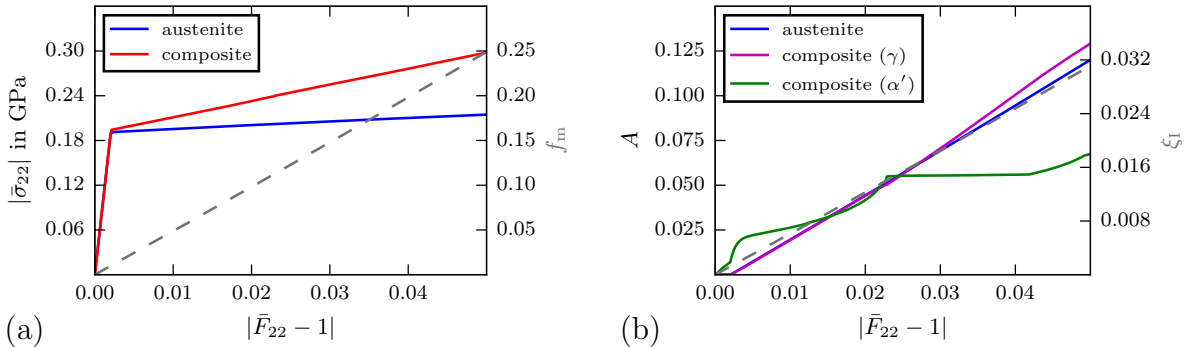


**Figure 3:** Comparison of the material response under uniaxial compression. (a) true stress-nominal strain curve of the two-phase composite material and the pure austenite and (b) evolution of the accumulated plastic slip  $A = \sum_{\alpha} \varepsilon_{\alpha}$  in the individual phases of the composite material and the pure austenite.

## 5 CONCLUSION

The current contribution describes a two-phase mean-field homogenization approach, employing an extended finite deformation Mori-Tanaka scheme. It accounts for additional stress-free eigenvelocity gradients associated with twinning or phase transformation in austenitic steels at the single crystal scale. In order to incorporate the eigenvelocity gradient into the rate-type formulation of the homogenization approach, a regularization of the former is proposed, which approximates the jump-like prescription of the deformation associated with the microstructural changes as soon as a transformed or twinned domain appears. The material behavior of the individual phases is captured by a finite strain crystal plasticity model, taking into account both anisotropic elastic and anisotropic plastic flow and hardening behavior. The mean-field model is employed in a uniaxial tension and uniaxial compression test with a prescribed evolution of multiple martensite variants developing inside the martensitic inclusion phase. It is found that there is a pronounced strengthening compared to the pure stable austenite, which is due to evolution of the martensitic phase and is consistent with experiments. Furthermore, a strong interaction between phase transformation and plasticity within the martensitic phase as well as a mutual interaction of the plastic deformation in the individual phases is observed. The latter also changes dynamically during the deformation process. As these complex interactions are not prescribed a priori and are rather due the adopted mean-field approach in conjunction with the constitutive models of the individual phases, the current modeling approach seems to be suitable to accurately describe the deformation behavior of austenitic steels at the single crystal scale. The current framework should be extended to incorporate a thermodynamically consistent transformation criterion. Such an extended model would allow for a critical assessment of the necessary complexity of plastic inheritance approaches.

## Acknowledgement

The authors gratefully acknowledge the Deutsche Forschungsgemeinschaft (DFG, German Research Foundation) for funding the research in the framework of the Collaborative Research Center “TRIP-Matrix Composites”, (project number 54473466 – SFB 799, sub-

project C10).

## REFERENCES

- [1] Martin, S., Wolf, S. Decker, S., Krüger, L. and Martin, U. Deformation Bands in High-Alloy Austenitic 16Cr6Mn6Ni TRIP Steel: Phase Transformation and Its Consequences on Strain Hardening at Room Temperature. *Steel Res. Int.* (2015) **86**:1187–1196.
- [2] Hallberg, H., Håkansson, P. and Ristinmaa, M. A Constitutive Model for the Formation of Martensite in Austenitic Steels under Large Strain Plasticity. *Int. J. Plasticity* (2007) **23**:1213–1239.
- [3] Seupel, A. and Kuna, M. Phenomenological Modeling of Strain Hardening, Phase Transformation and Damage Effects of TRIP-Steels. In: *Proceedings of XIV International Conference on Computational Plasticity COMPLAS* (2017) Barcelona, Spain p.576–587
- [4] Prüger, S., Seupel, A. and Kuna, M. A Thermomechanically Coupled Material Model for TRIP-Steel. *Int. J. Plasticity* (2014) **55**:182–197.
- [5] Cherkaoui, M., Souлами, A., Zeghloul, A. and Khaleel, M.A. A Phenomenological Dislocation Theory for Martensitic Transformation in Ductile Materials: From Micro to Macroscopic Description. *Philos. Mag.* (2008) **88**:3479–3512.
- [6] Kalidindi, S.R. Incorporation of Deformation Twinning in Crystal Plasticity Models. *J. Mech. Phys. Solids* (1998) **46**:267–290.
- [7] Roters, F. et al. DAMASK – The Düsseldorf Advanced Material Simulation Kit for Modeling Multi-Physics Crystal Plasticity, Thermal, and Damage Phenomena from the Single Crystal up to the Component Scale. *Comp. Mater. Sci.* (2019) **158**:420–478.
- [8] Levitas, V.I. Thermomechanical Theory of Martensitic Phase Transformations in Inelastic Materials. *Int. J. Solids Struct.* (1998) **35**:889–940.
- [9] Tjahjanto, D.D., Turteltaub, S. and Suiker, A.S.J. Crystallographically Based Model for Transformation-Induced Plasticity in Multiphase Carbon Steels. *Continuum Mech. Thermodyn.* (2008) **19**:399–422.
- [10] Feng, Z., Zecevic, M. and Knezevic, M. Stress-Assisted ( $\gamma \rightarrow \alpha'$ ) and Strain-Induced ( $\gamma \rightarrow \epsilon \rightarrow \alpha'$ ) Phase Transformation Kinetics Laws Implemented in a Crystal Plasticity Model for Predicting Strain Path Sensitive Deformation of Austenitic Steels. *Int. J. Plasticity* (2021) **136**:102807.
- [11] Wang, H. et al. Effect of Martensitic Phase Transformation on the Behavior of 304 Austenitic Stainless Steel under Tension. *Mat. Sci. Eng. A-Struct.* (2016) **649**:174–183.

- [12] Cherkaoui, M., Berveiller, M. and Sabar, H. Micromechanical Modeling of Martensitic Transformation Induced Plasticity (TRIP) in Austenitic Single Crystals. *Int. J. Plast.* (1998) **14**:597–626.
- [13] Kouznetsova, V.G. and Geers, M.G.D. A Multi-Scale Model of Martensitic Transformation Plasticity. *Mech. Mater.* (2008) **40**:641–657.
- [14] Eshelby, J.D. The Determination of the Elastic Field of an Ellipsoidal Inclusion, and Related Problems. *Proc. R. Soc. Lon. Ser.-A.* (1957) **241**:376–396.
- [15] Qu, J. and Cherkaoui, M. *Fundamentals of Micromechanics of Solids*. John Wiley & Sons, Inc., (2006).
- [16] Nemat-Nasser, S. Averaging Theorems in Finite Deformation Plasticity. *Mech. Mater.* (1999) **31**:493–523.
- [17] Mori, T. and Tanaka, K. Average Stress In Matrix and Average Elastic Energy of Materials With Misfitting Inclusions. *Acta Metall. Mater.* (1973) **21**:571–574.
- [18] Doghri, I., Ghezal, M.I. El and Adam, L. Finite Strain Mean-Field Homogenization of Composite Materials with Hyperelastic-Plastic Constituents. *Int. J. Plasticity* (2016) **81**:40–62.
- [19] Ponte Castañeda, P. and Suquet, P. Nonlinear Composites. *Adv. Appl. Mech.* (1998) **34**:172–302.
- [20] Willis, J.R. Bounds and Self-Consistent Estimates for the Overall Properties of Anisotropic Composites. *J. Mech. Phys. Solids* (1977) **25**:185–202.
- [21] Iwakuma T. and Nemat-Nasser S. Finite Elastic-Plastic Deformation of Polycrystalline Metals. *Proc. R. Soc. Lond. A* (1984) **394**:87–119.
- [22] Tanaka, M., Fujikawa, M., Balzani, D. Schröder, J. Robust Numerical Calculation of Tangent Moduli at Finite Strains Based on Complex-Step Derivative Approximation and Its Application to Localization Analysis. *Comput. Method. Appl. M.* (2014) **269**:454–470.
- [23] Bowles, J.S. and Mackenzie, J.K. The Crystallography of Martensite Transformations I. *Acta Metall. Mater.* (1954) **2**:129–137.
- [24] Wechsler, M.S. and Lieberman, D.S. and Read, T.A. On the Theory of the Formation of Martensite. *JOM-J. Met.* (1953) **197**:1503–1515.
- [25] Cayron, C. Continuous Atomic Displacements and Lattice Distortion during Fcc–Bcc Martensitic Transformation. *Acta Mater.* (2015) **96**:189–202.
- [26] Levitas, V.I., Idesman, A.V., Olson, G.B. and Stein, E. Numerical Modelling of Martensitic Growth in an Elastoplastic Material. *Philos. Mag. A* (2002) **82**:429–462.

- [27] Lani, F., Furnémont, Q., Van Rompaey, T., Delannay, F., Jacques, P.J. and Pardoën, T. Multiscale Mechanics of TRIP-Assisted Multiphase Steels: II. Micromechanical Modelling. *Acta Mater.* (2007) **55**:3695–3705.
- [28] Mahnken, R. Anisotropy in Geometrically Non-Linear Elasticity with Generalized Seth Hill Strain Tensors Projected to Invariant Subspaces. *Commun. Numer. Meth. Engng.* (2005) **21**:405–418.
- [29] Méric, L. and Cailletaud, G. Single Crystal Modeling for Structural Calculations: Part 2—Finite Element Implementation. *J. Eng. Mater.-T. ASME* (1991) **113**:171–182.
- [30] Peirce, D., Asaro, R.J. and Needleman, A. An Analysis of Nonuniform and Localized Deformation in Ductile Single Crystals. *Acta Metall.* (1982) **30**:1087–1119.
- [31] Prüger, S. and Kiefer, B. A Comparative Study of Integration Algorithms for Finite Single Crystal (Visco-)Plasticity. *Int. J. Mech. Sci.* (2020) **180**:105740.
- [32] Prüger, S. and Kiefer, B. Towards the Crystal Plasticity Based Modeling of TRIP-Steels—From Material Point to Structural Simulations. In Biermann, H. and Aneziris, C. G. (Eds.), *Austenitic TRIP/TWIP Steels and Steel-Zirconia Composites: Design of Tough, Transformation-Strengthened Composites and Structures*, pp.793–823, Springer International Publishing, 2020.
- [33] Karaman, I., Sehitoglu, H., Maier, H.J. and Chumlyakov, Y.I. Competing Mechanisms and Modeling of Deformation in Austenitic Stainless Steel Single Crystals with and without Nitrogen. *Acta Mater.* (2001) **49**:3919–3933.
- [34] Keh, A.S. Work Hardening and Deformation Sub-Structure in Iron Single Crystals Deformed in Tension at 298°K. *Philos. Mag.* (1965) **12**:9–30.
- [35] Renner, E., Gaillard, Y., Richard, F., Amiot, F. and Delobelle, P. Sensitivity of the Residual Topography to Single Crystal Plasticity Parameters in Berkovich Nanoindentation on FCC Nickel. *Int. J. Plasticity* (2016) **77**:118–140.
- [36] Zambaldi, C., Yang, Y., Bieler, T.R. and Raabe, D. Orientation Informed Nanoindentation of  $\alpha$ -Titanium: Indentation Pileup in Hexagonal Metals Deforming by Prismatic Slip. *J. Mater. Res.* (2012) **27**:356–367.
- [37] Ledbetter, H.M. Monocrystal-Polycrystal Elastic Constants of a Stainless Steel *Phys. Status Solidi A* (1984) **85**:89–96.
- [38] Ledbetter, H. and Kim, S. *Handbook of Elastic Properties of Solids, Liquids and Gases*. Academic Press, Vol. II., (2001).
- [39] Guery, A., Hild, F., Latourte, F. and Roux, S. Identification of Crystal Plasticity Parameters Using DIC Measurements and Weighted FEMU. *Mech. Mater.* (2016) **100**:55–71.